



**HAL**  
open science

# The brightness ratio of H Lyman- $\alpha$ /H 2 bands in FUV auroral emissions: A diagnosis for the energy of precipitating electrons and associated magnetospheric acceleration processes applied to Saturn

Chihiro Tao, Laurent Lamy, Renée Prangé

## ► To cite this version:

Chihiro Tao, Laurent Lamy, Renée Prangé. The brightness ratio of H Lyman-  $\alpha$  /H 2 bands in FUV auroral emissions: A diagnosis for the energy of precipitating electrons and associated magnetospheric acceleration processes applied to Saturn. *Geophysical Research Letters*, 2014, 41 (19), pp.6644-6651. 10.1002/2014GL061329 . hal-02544434

**HAL Id: hal-02544434**

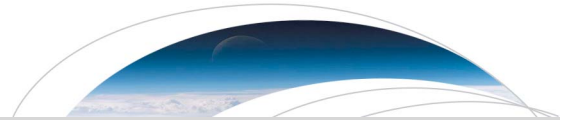
**<https://hal.science/hal-02544434>**

Submitted on 11 Oct 2021

**HAL** is a multi-disciplinary open access archive for the deposit and dissemination of scientific research documents, whether they are published or not. The documents may come from teaching and research institutions in France or abroad, or from public or private research centers.

L'archive ouverte pluridisciplinaire **HAL**, est destinée au dépôt et à la diffusion de documents scientifiques de niveau recherche, publiés ou non, émanant des établissements d'enseignement et de recherche français ou étrangers, des laboratoires publics ou privés.

Copyright



## RESEARCH LETTER

10.1002/2014GL061329

## Key Points:

- H Lyman- $\alpha$ /H<sub>2</sub> brightness ratio is a good indicator for auroral electron energy
- Electron flux-energy relation is obtained from observed Saturn FUV brightness
- Acceleration and nonacceleration processes of auroral electrons are discussed

## Correspondence to:

C. Tao,  
chihiro.tao@irap.omp.eu

## Citation:

Tao, C., L. Lamy, and R. Prangé (2014), The brightness ratio of H Lyman- $\alpha$ /H<sub>2</sub> bands in FUV auroral emissions: A diagnosis for the energy of precipitating electrons and associated magnetospheric acceleration processes applied to Saturn, *Geophys. Res. Lett.*, *41*, 6644–6651, doi:10.1002/2014GL061329.

Received 2 AUG 2014

Accepted 25 SEP 2014

Accepted article online 29 SEP 2014

Published online 14 OCT 2014

## The brightness ratio of H Lyman- $\alpha$ /H<sub>2</sub> bands in FUV auroral emissions: A diagnosis for the energy of precipitating electrons and associated magnetospheric acceleration processes applied to Saturn

Chihiro Tao<sup>1</sup>, Laurent Lamy<sup>2</sup>, and Renée Prangé<sup>2</sup>

<sup>1</sup>IRAP, Université de Toulouse/UPS-OMP/CNRS, Toulouse, France, <sup>2</sup>LESIA, Observatoire de Paris, CNRS, UPMC, Université Paris Diderot, Meudon, France

**Abstract** We propose that the ratio of the auroral brightness of H Lyman- $\alpha$  to that of far ultraviolet H<sub>2</sub> and the absolute value of the H<sub>2</sub> brightness provide good indicators of the acceleration versus nonacceleration processes for field-aligned auroral electron precipitation in the Saturn magnetosphere-ionosphere coupled system. This finding is based on model results indicating that this ratio is a decreasing function of the auroral electron energy over the whole auroral energy range, as previously suggested by Cassini observations. For electron energies above 5 keV, the results agree with the Knight relation, as in the environments of the Earth and Jupiter. On the other hand, decreasing electron flux with increasing electron energies below a few keV is also found and alternately explained as a nonacceleration reflecting the magnetospheric plasma distribution and/or wave-particle interactions.

### 1. Introduction

The far ultraviolet (FUV) emissions in the H<sub>2</sub>-dominated atmosphere of the outer planets visualize energy-release processes in their coupled magnetosphere-ionosphere-thermosphere system. Since the emissions are radiated from H<sub>2</sub> and H species excited by precipitating energetic particles, they contain information about the precipitating particles such as their input energy flux and particle energy (see the review of *Badman et al.* [2014], and references therein).

The auroral particle energy flux and energy are key parameters that allow to infer the nature of the electron precipitating process. *Knight* [1973] modeled the relationship between the current flowing up terrestrial auroral magnetic field lines and the auroral electron energy accelerated by field-aligned (FA) potential drops.

The FA current-voltage relation estimated from a Vlasov model applied to Jupiter, at and beyond the orbit of I<sub>o</sub>, indicates that the FA currents are limited due to the plasma confinement by a centrifugal force and the onset of a resulting ambipolar potential drop, and that it must deviate from the Knight relation [e.g., *Ray et al.*, 2009]. Applying this model to Saturn, *Ray et al.* [2012, 2013] revealed less confinement due to the lower mass and larger abundance of light ions in Saturn's magnetosphere than in Jupiter's. It was suggested that the acceleration processes on the Kronian auroral field lines may be due to FA potential drops with a relation consistent with that predicted for Earth by *Knight* [1973].

The auroral emissions provide proxies of the FA current and electron energy by means of the observed emission brightness and its "FUV color ratio (CR)," defined as the ratio of the intensity of a waveband unabsorbed by hydrocarbons to that of an absorbed one, and used in combination with a model of atmosphere. The CR is routinely used for Jupiter where the auroral source is most embedded within the hydrocarbons layer. The electrons can reach lower altitudes with increasing electron energy, hence the CR increases with electron energy. Using this method for observed Jovian aurorae, *Gustin et al.* [2004] revealed a positive correlation between the electron energy (30–200 keV) and the electron flux density ( $\sim 0.04$ – $0.4 \mu\text{A m}^{-2}$ ) in the form of a square root law, and they explained this dependence using the Knight's acceleration theory.

For Saturn, the hydrocarbon absorption is always weak or undetectable on the H<sub>2</sub> spectra, leading to inferences that the precipitating electrons are much lower energy, up to a few tens of keV [e.g., *Gustin et al.*, 2009];

Lamy *et al.*, 2013, hereafter referred to as L13]. Therefore, the CR cannot always be used to establish relations between auroral electron energy and electron flux on Saturn. However, a recent analysis of Saturn's southern aurorae with the Ultraviolet Imaging Spectrograph on board Cassini established that the brightness ratio of H Lyman- $\alpha$  to FUV H<sub>2</sub> auroral emissions (hereafter referred to as H/H<sub>2</sub> brightness ratio) statistically decreases with increasing brightness of H<sub>2</sub> [L13] and suggested that the latter is positively correlated with the energy of the precipitating electrons. This observational quantity was thus proposed as a sensitive proxy for low-energy electrons in a range where the usual CR indicator becomes insensitive (typically <10 keV). However, since the H<sub>2</sub> brightness also depends on the electron flux, their result indicates that the electron energy and flux variation should be limited within a certain range. Previous models of auroral energy deposition [e.g., Rego *et al.*, 1999] also predicted a decrease of this brightness ratio with increasing electron energy.

In order to investigate the nature of the precipitating electrons driving aurora on Saturn, we thus establish the conversion relation from observed H and H<sub>2</sub> brightness into auroral electron energy and electron flux using auroral emission models as described in section 2. Applying the conversion relation to the observed auroral brightness by L13, we derive the electron energy and flux relation for Saturn in section 3. Section 4 discusses characteristic relations seen in the results, followed by conclusions in section 5.

## 2. Model and Brightness Estimation

### 2.1. Model and Estimation

In order to convert the observed H and H<sub>2</sub> auroral brightnesses into a relation between electron energy (voltage) and flux (current), we use the auroral H Lyman- $\alpha$  emission model by Menager *et al.* [2010] and the H<sub>2</sub> emission model by Tao *et al.* [2011]. The relevance of the combined use of these two models is discussed later.

Menager *et al.* [2010] used a multistream electron transport code solving the 1-D Boltzmann equation to obtain the excitation rates of H<sub>2</sub>, CH<sub>4</sub>, and H(2p) (including quenching of the metastable H(2s) level) due to collisions of primary and secondary electrons in the H<sub>2</sub>-dominated atmosphere of Jupiter. In addition to the photoexcitation of H<sub>2</sub> and CH<sub>4</sub>, the transition associated with Lyman- $\alpha$  emission is also considered. Then, a radiative transfer code is used to calculate the emergent intensity and line profile including the scattering of Lyman- $\alpha$  photons by atmospheric H atoms. All steps of the process are dependent on the incident electron energy, either directly or indirectly through the vertical distribution of the atmospheric species (i.e., the Lyman- $\alpha$  produced mainly from H<sub>2</sub> dissociation at low-altitude by high energy electrons and from direct H excitation at high altitude by low energy electrons). For a fixed electron energy influx of 11 mW m<sup>-2</sup> and several characteristic energies (i.e., half of the mean energy of the Maxwellian distribution) of 0.1, 1, 10, 30, 50, 100, and 150 keV, Menager *et al.* [2010] estimated the Lyman- $\alpha$  line brightness to be 101, 63.2, 14.9, 3.02, 1.18, 0.385, and 0.174 kR, respectively. Assuming that brightness is proportional to the auroral electron flux, we can plot the contours of the Lyman- $\alpha$  brightness as a function of the electron energy and of the electron flux (Figure 1a).

We estimate the H<sub>2</sub> brightness following Tao *et al.* [2011], who estimated the excitation of the H<sub>2</sub> bands by electron impact using a Monte Carlo-type electron transfer code [Hiraki and Tao, 2008]. The H<sub>2</sub> brightness isocontours summed up over the 80–170 nm wavelength range are plotted in Figure 1b as functions of the electron characteristic energy and total flux of the Maxwellian spectra. The electron flux is then converted into current density ( $\mu\text{A m}^{-2}$ ). For example, it can be seen from the figure that a characteristic incident energy of 5 keV or a mean energy of 10 keV with an electron flux of 0.1  $\mu\text{A m}^{-2}$ , which corresponds to 1 mW m<sup>-2</sup> input power, produces 10 kR of total H<sub>2</sub> emission. This is consistent with the  $\sim 10$  kR per mW m<sup>-2</sup> conversion factor proposed by other model studies [e.g., Gérard and Singh, 1982; Waite *et al.*, 1983; Grodent *et al.*, 2001]. This relation (shown by dashed line) does not take into account any hydrocarbon absorption. The actual brightness contour considering the hydrocarbon absorption overlying the emission source (solid line) deviates from this relation for electron energies exceeding 30 keV.

Figure 1c displays the resulting contours of the H/H<sub>2</sub> brightness ratio. Since the H<sub>2</sub> FUV brightness is also almost proportional to the electron flux, the brightness ratio does not depend on the electron flux. This ratio decreases with increasing electron energy as shown in Figure 1d. Hence, we can estimate electron energy from the brightness ratio. It is a very sensitive diagnostic tool below  $\sim 10$  keV where it varies from 1 to 0.1, while it tends asymptotically toward zero above  $\sim 30$  keV. From the dependence of the ratio on energy,

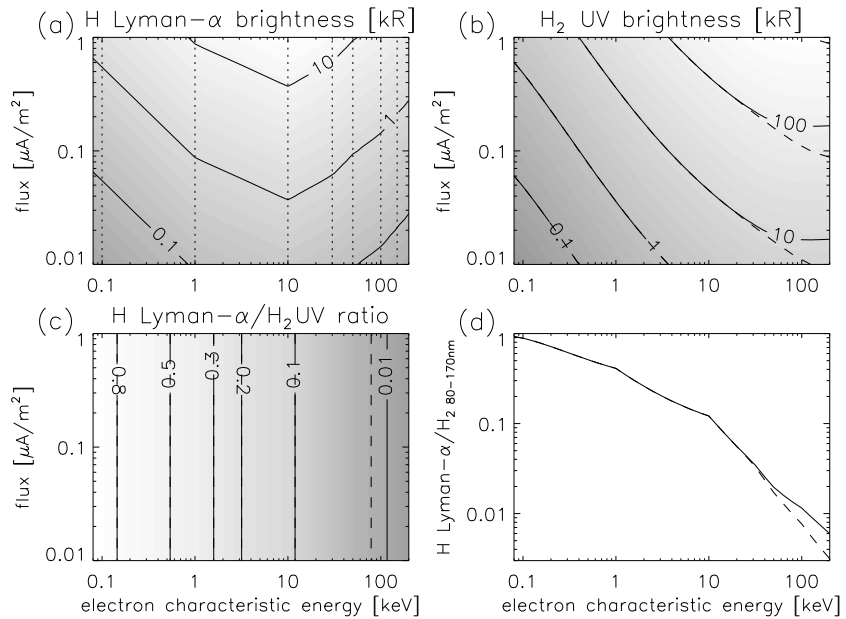


**Figure 1.** Contours of (a) H Lyman- $\alpha$  brightness, (b) H<sub>2</sub> brightness over 80–170 nm, and (c) the ratio of Lyman- $\alpha$  to H<sub>2</sub> 80–170 nm brightness, as functions of electron characteristic energy and flux, and (d) the ratio as a function of electron characteristic energy, estimated from models. Vertical dotted lines in Figure 1a show the energy listed in Table 6 of Menager *et al.* [2010]. The solid (dashed) lines in Figures 1b–1d show the values derived using the H<sub>2</sub> brightness with (without) hydrocarbon absorption.

$dW_{\text{chara}}/W_{\text{chara}} = 0.5$  is achieved by a signal-to-noise ratio (SNR) of  $\sim 10$  for the energy range  $0.1 < W_{\text{chara}} < 10$  keV, assuming the same SNR for H<sub>2</sub> and H brightnesses for simplicity. Observations by L13 applied here have sufficient SNR.

This energy estimation was suggested previously by Rego *et al.* [1999] using electron energy degradation and radiation transfer models. Using the same H<sub>2</sub> wavelength range (123–130 nm), we confirm the dependence of the ratio on electron energy, namely a monotonic increase with energy. Our results quantitatively differ from those of Rego *et al.* [1999] (Figure 2) within the difference in H Lyman- $\alpha$  line profile owing to different atmosphere models as discussed in Menager *et al.* [2010].

**2.2. Limitations and Evaluation**

Here several limitations on the model estimations must be discussed. First, we have combined two different emission models, based on two different atmospheric models: that of Jupiter for H Lyman- $\alpha$  and that of Saturn for H<sub>2</sub>. As a consequence, the brightness ratio is expected to vary with the neutral H density profiles as a function of the H<sub>2</sub> column density. However, since H production and loss reactions are related to H<sub>2</sub> through electron collisions and photoionizations, the relation between the H profile and H<sub>2</sub> column density is expected to be similar for H<sub>2</sub>-dominated planets such as Jupiter and Saturn. Since we refer to altitude-integrated brightness values, the effects due to the different scale heights of the two planets would be negligible.

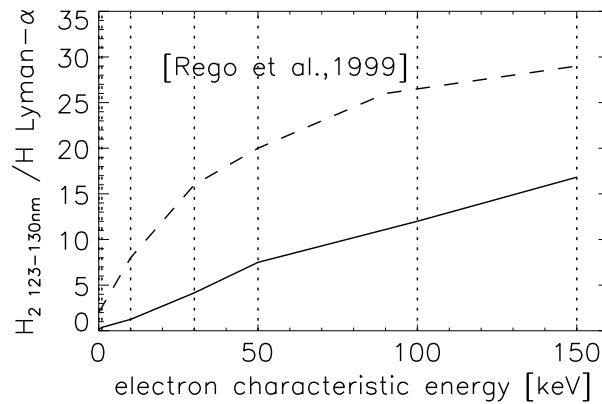


**Figure 2.** The ratio of H<sub>2</sub> brightness over 123–130 nm to H Lyman- $\alpha$  as a function of electron characteristic energy. Dashed line shows those obtained by Rego *et al.* [1999]. Vertical dotted lines show the energy listed in Table 6 of Menager *et al.* [2010].

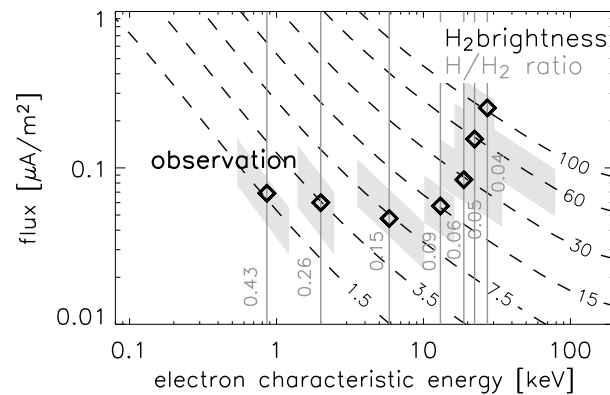


**Figure 3.** Observed points (their variable ranges) shown by diamonds (gray shades) as functions of electron characteristic energy and flux. Dashed and solid lines show contours of the  $H_2$  brightness and the  $H/H_2$  brightness ratio, respectively.

particular on the H distribution, and on its response to the auroral energy input, as investigated for Jupiter by several previous studies. *Waite et al.* [1983] estimated this effect by computing the extra production of H atoms and the Lyman- $\alpha$  production with a self-consistent model. The ratio of the energy deposited into the Jovian auroral Lyman- $\alpha$  line and into the  $H_2$  Lyman and Werner bands varied from 0.28 (0.27) without atmospheric feedback to 0.34 (0.94) with feedback for 10 (1) keV primary electrons, respectively. This suggests that the variability of the Jovian atmosphere due to auroral precipitations may increase the Lyman- $\alpha$  production rate especially for low-energy primary electrons. On the other hand, this may be largely diminished through increased attenuation by radiative transfer by the denser overlying H populations. Indeed, for Jupiter, *Rego et al.* [1994] and *Menager et al.* [2010] indicate that the use of atmospheric models where the H distribution varies by a factor of  $< \sim 10$  affects the H Lyman- $\alpha$  brightness by up to  $\sim 50\%$ . Despite this discrepancy, the trend of decreasing ratio with increasing electron energy remains the same among models, including also a different model setting by *Yung et al.* [1982]. In addition, for the Saturn case of interest here, this feedback effect seems smaller due to the smaller energy input,  $\sim 0.1$  to a few  $mW m^{-2}$  [e.g., *Cowley et al.*, 2008], compared to that of Jupiter,  $\sim 2\text{--}200 mW m^{-2}$  [e.g., *Prangé et al.*, 1998; *Gustin et al.*, 2004]. Fourth, precipitation of ions with emission lines in these spectral ranges might slightly modify the ratio as investigated for Jupiter [*Waite et al.*, 1988]. However, ion precipitations are not expected so far for Saturn.

The use of different atmospheric models and the corresponding model uncertainties would modify the absolute value of the ratio by several 10s% as seen above, while it is well within the observation variances (several 10s% to a few factors as in section 3). L13 provided evidence of the applicability of the Lyman- $\alpha$  brightness ratio to the energy estimation. Their Figure 6 shows that the observed  $H/H_2$  brightness ratio remains within a small range for any  $H_2$  brightness step even though data are collected from various spatial (over northern auroral region) and temporal (one night, including a bright injection event) locations. They simultaneously found in the observed aurora that the  $H/H_2$  brightness ratio decreases with increasing CR (i.e., electron energy) in the high-energy range where the latter is usable.

### 3. Determination of Energy and Flux of the Precipitating Electrons

At this point, we will derive quantitatively the electron energy to electron input flux relation based on the observed  $H/H_2$  brightness ratio to  $H_2$  brightness [L13]. We can then overplot on the same coordinate system of precipitating auroral electron energy and flux for the contours of (i) the  $H/H_2$  brightness ratio and (ii) the  $H_2$  brightness, as estimated in section 2 and plotted separately in Figures 1c and 1b. Since these parameters have different dependences on energy and flux, each set of parameters at the crossing of two (i) and (ii) isocontours defines a unique parameters set of precipitating electron energy and flux (Figure 3). L13 derived a series of such pairs of (i) and (ii) quantities in their Figure 7a and Table 1. Once they are plotted over Figure 3 (diamonds), we obtain the parameters of the electrons responsible for these Kronian aurora. The parameters define a curve in the electron energy-electron flux coordinate system for which the electron flux first decreases with increasing electron

Second, the H line is also absorbed by the hydrocarbons as modeled by *Gustin et al.* [2013], while here this effect is not considered. Since the hydrocarbons are located at low altitudes, this would result in overestimation of electron energies in the high-energy electron range only ( $> \sim 30$  keV for  $H_2$  total brightness referring Figure 1b). Since this value is larger than the typical auroral electron energy at Saturn, which is estimated to be 10–30 keV [e.g., *Gérard et al.*, 2009] and those obtained in the next section, our assumption is therefore valid over 10–30 keV, and not necessary below 10 keV, where absorption is not observed.

The H Lyman- $\alpha$  brightness depends on the vertical atmospheric composition, in

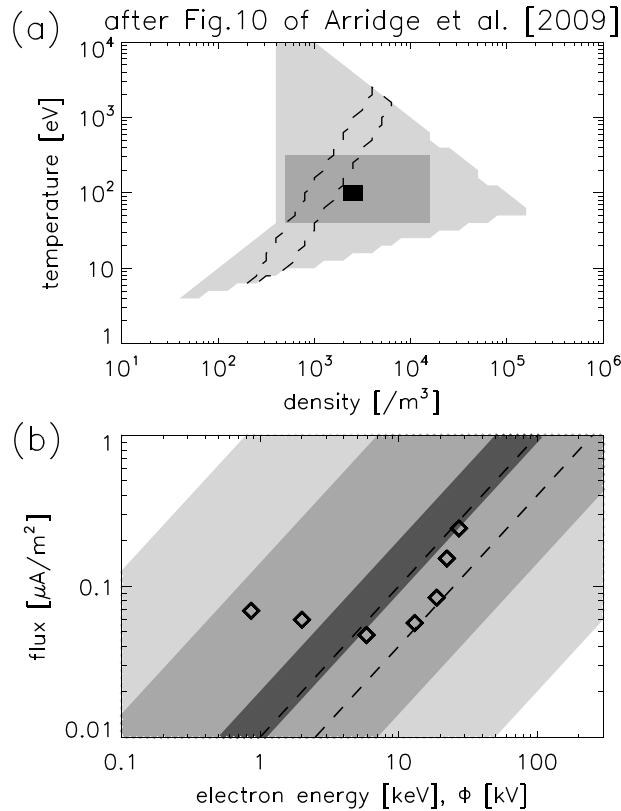


**Figure 4.** (a) Sample map of electron temperature as a function of electron density from Cassini/EPD observation [after *Arridge et al., 2009*] and (b) variable ranges of electron energy and flux related by the Knight relation. Light, moderate, and dark gray contours in Figure 4a indicate the number of samples by the EPD, ranging 1–10, 10–200, and >200, respectively. The region surrounded by dashed line is from the observed values, diamonds, at >5 keV in Figure 4b.

energy (from a current of  $0.07 \mu\text{A m}^{-2}$  or a particle flux density of  $4.4 \times 10^{17} \text{ m}^{-2}$  for electrons of 0.9 keV to  $0.045 \mu\text{A m}^{-2}$  or  $2.8 \times 10^{17} \text{ m}^{-2}$  for 5 keV); and after a minimum between 5 and 10 keV, the electron flux increases with increasing electron energy (from a current of  $0.055 \mu\text{A m}^{-2}$  or a particle flux density of  $3.4 \times 10^{17} \text{ m}^{-2}$  for electrons of 11 keV to  $0.215 \mu\text{A m}^{-2}$  or  $13.5 \times 10^{17} \text{ m}^{-2}$  for 27 keV). Note that the observations in the high-energy range mainly correspond to sources located in the bright main oval as shown in Figure 4 of L13.

#### 4. Discussion: Use of the Auroral Emission as a Diagnosis of the Precipitation Processes

Since the electron parameters above are derived from auroral observations, they characterize the electron beams at the top of the atmosphere and must thus reflect the physical processes responsible for their precipitation, either diffusion in the phase space or FA acceleration. We discuss the relationship between the auroral electron energy-flux parameters and the presence of a FA acceleration process at Saturn in this section.

##### 4.1. Relation From the Knight Theory

We assume that the theory modeling the acceleration of the terrestrial

auroral electron beams [Knight, 1973] is applicable to the Saturn magnetospheres as proposed by Ray et al. [2013] by using a kinetic Vlasov model.

The maximum value of the upward FA current density measured just above the ionosphere  $j_{//0}$  that can be carried by precipitating magnetospheric electrons without FA acceleration is

$$j_{//0} = eN \left( \frac{W_{\text{th}}}{2\pi m_e} \right)^{1/2}, \quad (1)$$

where  $e$  and  $m_e$  are the charge and mass of the electron, respectively,  $N$  and  $W_{\text{th}} = k_B T$  are the number density and thermal energy of the magnetospheric electron population assumed to have an isotropic Maxwellian distribution with temperature  $T$ , respectively, and  $k_B$  is the Boltzmann constant. Under the approximation of the infinite mirror ratio case, the potential drop  $\Phi_{//}$  along the field line required to reach the necessary current density  $j_{//}$  outside of the ionosphere is [Cowley and Bunce, 2001; Gustin et al., 2004]

$$e\Phi_{//} = W_{\text{th}} \left[ \left( \frac{j_{//}}{j_{//0}} \right) - 1 \right], \quad (2)$$

and the enhanced energy flux of precipitating electron becomes

$$E_f = \frac{E_{f_0}}{2} \left[ \left( \frac{j_{//}}{j_{//0}} \right)^2 + 1 \right], \quad (3)$$

where the  $E_{f0}$  is the energy flux without FA acceleration,

$$E_{f0} = 2NW_{th} \left( \frac{W_{th}}{2\pi m_e} \right)^{1/2}. \quad (4)$$

Using the relations, the mean energy of the precipitating electrons  $\langle W \rangle$  can be obtained as

$$\langle W \rangle = \frac{E_f}{j_{//}} = 2W_{th} \frac{E_f/E_{f0}}{j_{//}/j_{//0}} = W_{th} \frac{\left( j_{//}/j_{//0} \right)^2 + 1}{j_{//}/j_{//0}} \quad (5)$$

which can be approximated using  $j_{//} \gg j_{//0}$ , as

$$\langle W \rangle \sim W_{th} j_{//}/j_{//0}. \quad (6)$$

Then using the characteristic energy of the Maxwellian distribution,

$$j_{//} \sim \frac{j_{//0}}{W_{th}} \langle W \rangle = \frac{j_{//0}}{W_{th}} 2W_{th} W_{chara} = \frac{2eN}{(2\pi m_e k_B T)^{1/2}} W_{chara}. \quad (7)$$

This relation relates linearly the current density (i.e., the electron flux) to the characteristic energy of the accelerated electron beam at the top of the atmosphere by a factor which depends on the magnetospheric plasma density  $N$  and temperature  $T$ .

*Arridge et al.* [2009] have performed a statistical analysis of the Cassini Energetic Particle Detector (EPD) in the Saturn midnight-to-dawn lobes and the central and outer plasma sheet at  $>15 R_s$ , from which they have derived a map of the electron temperature as a function of electron density in their Figure 10, schematically represented here in Figure 4a. Light, moderate, and dark gray contours indicate the number of samples detected by the EPD ranging 1–10, 10–200, and  $>200$ , respectively. In the inner magnetosphere at radial distances of 2.8–10  $R_s$ , a positive correlation between electron temperature (0.3–5 eV) and density (30–100  $\text{cm}^{-3}$ ) is estimated from the local plasma frequency observed by the Cassini/Radio and Plasma Wave Science instrument [*Schippers et al.*, 2013].

Using equation (6), this map can be converted into a diagram in the characteristic energy-current density (i.e., electron flux) space (Figure 4b). In the log-log scale used, the energy/flux contours are a series of lines parallel to the axes bisector,  $\log j_{//} = \log W_{chara} + \log \{2eN(2\pi m_e k_B T)^{-1/2}\}$ . We have overplotted the observation-derived auroral data using the diamonds from Figure 3, which, as discussed above, exhibit very different behaviors in the low- and high-energy regions. The agreement applies to the high-energy range as will be discussed in the next section.

#### 4.2. High-Energy Range (~10–30 keV)

Above ~10 keV, the electron energy flux derived from the auroral brightnesses by L13 roughly overlap lines ( $\log j_{//} - \log W_{chara}$ ) derived from the Knight relation with those observed magnetospheric parameters. This strongly suggests that the “high”-energy electron population precipitated into the aurorae of Saturn has been accelerated by FA potential drops. Inversely, the source density-temperature parameter range corresponding to the observed brightness is overplotted by dashed contour in Figure 4a. For the 100–200 eV electron energy range, a magnetospheric condition with  $\sim 10^3 \text{ m}^{-3}$  density (within the dashed line region) corresponds to the outer plasma sheet region according to Table 1 of *Arridge et al.* [2009].

#### 4.3. Low-Energy Range (~0.085–5 keV)

Below 5 keV, the observational data are practically perpendicular to the lines derived from the Knight relation. We thus infer that the corresponding electrons have not been precipitated by FA acceleration (potential drop). Electron temperature  $<0.3$  keV is quite frequently observed in the magnetosphere, as shown in the statistical analysis by *Arridge et al.* [2009] (Figure 4a). This shows that the electron flux generally decreases with electron energy at  $> \sim 0.3$  keV range, which is the same trend found in the observation-based parameter relation seen in Figure 3 in the  $<5$  keV range. This decreasing electron flux with increasing electron energy would directly reflect the original magnetospheric electron profile, which is one possible interpretation of this trend.

The precipitating electron energy spectrum can also be affected by the efficiency of pitch angle scattering in the magnetosphere. Whistler-mode chorus waves have been detected by previous observations and can resonate with electrons with energies from a few 100 eV to a few keV [Hospodarsky et al., 2008; Menietti et al., 2013]. Whistler-mode hiss waves are associated with the FA electron beam with energy of a few 100 eV [e.g., Kopf et al., 2010; Gurnett et al., 2011]. Radioti et al. [2009] explained the coexistence of magnetospheric energetic neutral atoms and bright UV auroral structures due to pitch angle scattering of electrons of ~10s keV by whistler waves during an injection event. Pitch angle scattering at Earth is associated with pulsating auroral patches which are seen in the substorm recovery phase. In addition to the applicability of terrestrial substorm physics to Saturn, the dependence of the scattering efficiency on electron energy and relation with the acceleration in detail are open questions.

The observed Enceladus footprint aurora and flickering electron beams near Enceladus are explained as multiple reflections of standing Alfvén wave by analogy to the Io footprint at Jupiter [Pryor et al., 2011]. The observed beam spectrum peaks at ~10 eV and ~1 keV, which would also contribute the electron energy and flux relation. The broadband auroral acceleration mechanism by inertial Alfvén waves would also affect the low-energy (<5 keV) range since the energy spectrum drops off above ~5 keV at Io wake [Frank and Paterson, 2000]. Hess et al. [2010, 2011] estimated that Alfvén wave filamentation leads to a precipitating electron power, which is consistent with the power of the observed UV footprints of Io, Europa, and Enceladus. Investigation of the brightnesses separating auroral structures and locations will require a future study to distinguish the effects of these different mechanisms.

## 5. Conclusions

Comparisons of models of the FUV auroral emission by magnetospheric electron impact on the atmosphere to Cassini observations have confirmed that the H/H<sub>2</sub> brightness ratio is a decreasing function of the precipitating electron energy. This function, which is particularly sensitive at low energies (<20 keV), can be a useful tool to estimate the electron energy in an energy range where analysis of the hydrocarbon absorption of the H<sub>2</sub> spectrum becomes insensitive.

We have then established a flux-energy relation for the precipitating electrons from the observation-derived H/H<sub>2</sub> brightness ratio and the H<sub>2</sub> brightness in the Saturn aurorae. This function exhibits two different behaviors below and above ~5 keV. Applied to a set of Cassini plasma data, we have shown that the high-energy-region behavior of the electron energy-flux function derived from the auroral FUV observations is likely to be produced by a potential drop-induced acceleration along the field lines. The low-energy-region behavior does not fulfill the FA acceleration conditions for the same magnetospheric source and may result from pitch angle scattering by whistler-mode waves and/or acceleration by Alfvén waves.

## Acknowledgments

This research was supported by a grant-in-aid for Scientific Research from the Japan Society for the Promotion of Science (JSPS). L.L. and R.P. are supported by CNES. C.T. thanks C.S. Arridge, H. Tadokoro, H. Melin, and Y. Miyoshi for their helpful discussions. We referred to observation results from Lamy et al. [2013] and Arridge et al. [2009].

W. K. Peterson thanks Dirk Lummerzheim and two anonymous reviewers for their assistance in evaluating this paper.

## References

- Arridge, C. S., et al. (2009), Plasma electrons in Saturn's magnetotail: Structure, distribution and energisation, *Planet. Space Sci.*, *509*, 2032–2047.
- Badman, S. V., G. Branduardi-Raymont, M. Galand, S. Hess, N. Krupp, L. Lamy, H. Melin, and C. Tao (2014), Auroral processes at the giant planets: Energy deposition, emission mechanisms, morphology and spectra, *Space Sci. Rev.*, doi:10.1007/s11214-014-0042-x.
- Cowley, S. W. H., and E. J. Bunce (2001), Origin of the main auroral oval in Jupiter's coupled magnetosphere-ionosphere system, *Planet. Space Sci.*, *49*, 1067–1088.
- Cowley, S. W. H., C. S. Arridge, E. J. Bunce, J. T. Clarke, A. J. Coates, M. K. Dougherty, J.-C. Gérard, D. Grodent, J. D. Nichols, and D. L. Talboys (2008), Auroral current systems in Saturn's magnetosphere: Comparison of theoretical models with Cassini and HST observations, *Ann. Geophys.*, *26*, 2613–2630.
- Frank, L. A., and W. R. Paterson (2000), Observations of plasmas in the Io torus with the Galileo spacecraft, *J. Geophys. Res.*, *105*(A7), 16,017–16,034, doi:10.1029/1999JA000250.
- Gérard, J.-C., and V. Singh (1982), A model of energy deposition of energetic electrons and EUV emission in the Jovian and Saturnian atmospheres and implications, *J. Geophys. Res.*, *87*, 4525–4532, doi:10.1029/JA087iA06p04525.
- Gérard, J.-C., B. Bonfond, J. Gustin, D. Grodent, J. T. Clarke, D. Bisikalo, and V. Shematovich (2009), Altitude of Saturn's aurora and its implications for the characteristic energy of precipitated electrons, *Geophys. Res. Lett.*, *36*, L02202, doi:10.1029/2008GL036554.
- Grodent, D., J. H. Waite Jr., and J.-C. Gérard (2001), A self-consistent model of the Jovian auroral thermal structure, *J. Geophys. Res.*, *106*(A7), 12,933–12,952, doi:10.1029/2000JA900129.
- Gurnett, D. A., et al. (2011), Auroral hiss, electron beams and standing Alfvén wave currents near Saturn's moon Enceladus, *Geophys. Res. Lett.*, *38*, L06102, doi:10.1029/2011GL046854.
- Gustin, J., J.-C. Gérard, D. Grodent, S. W. H. Cowley, J. T. Clarke, and A. Grard (2004), Energy-flux relationship in the FUV Jovian aurora deduced from HST-STIS spectral observations, *J. Geophys. Res.*, *109*, A10205, doi:10.1029/2003JA010365.
- Gustin, J., J.-C. Gérard, W. Pryor, P. D. Feldman, D. Grodent, and G. Holsclaw (2009), Characteristics of Saturn's polar atmosphere and auroral electrons derived from HST/STIS, FUSE and Cassini/UVIS spectra, *Icarus*, *200*, 176–187, doi:10.1016/j.icarus.2008.11.013.

- Gustin, J., et al. (2013), Effects of methane on giant planet's UV emissions and implications for the auroral characteristics, *J. Mol. Spectr.*, *291*, 108–117.
- Hess, S. L. G., P. Delamere, V. Dols, B. Bonfond, and D. Swift (2010), Power transmission and particle acceleration along the Io flux tube, *J. Geophys. Res.*, *115*, A06205, doi:10.1029/2009JA014928.
- Hess, S. L. G., P. A. Delamere, V. Dols, and L. C. Ray (2011), Comparative study of the power transferred from satellite-magnetosphere interactions to auroral emissions, *J. Geophys. Res.*, *116*, A01202, doi:10.1029/2010JA015807.
- Hiraki, Y., and C. Tao (2008), Parameterization of ionization rate by auroral electron precipitation in Jupiter, *Ann. Geophys.*, *26*, 77–86.
- Hospodarsky, G. B., T. F. Averkamp, W. S. Kurth, D. A. Gurnett, J. D. Meniotti, O. Santolik, and M. K. Dougherty (2008), Observations of chorus at Saturn using the Cassini Radio and Plasma Wave Science instrument, *J. Geophys. Res.*, *113*, A12206, doi:10.1029/2008JA013237.
- Knight, S. (1973), Parallel electric fields, *Planet. Space Sci.*, *21*, 741–750.
- Kopf, A. J., et al. (2010), Electron beams as the source of whistler-mode auroral hiss at Saturn, *Geophys. Res. Lett.*, *37*, L09102, doi:10.1029/2010GL042980.
- Lamy, L., R. Prangé, W. Pryor, J. Gustin, S. V. Badman, H. Melin, T. Stallard, D. G. Mitchell, and P. C. Brandt (2013), Multispectral simultaneous diagnosis of Saturn's aurorae throughout a planetary rotation, *J. Geophys. Res. Space Physics*, *118*, 4817–4843, doi:10.1002/jgra.50404.
- Menager, H., M. Barthélemy, and J. Liliensten (2010), H Lyman  $\alpha$  line in Jovian aurora: Electron transport and radiative transfer coupled modeling, *Astron. Astrophys.*, *509*, A56.
- Meniotti, J. D., P. Schippers, Y. Katoh, J. S. Leisner, G. B. Hospodarsky, D. A. Gurnett, and O. Santolik (2013), Saturn chorus intensity variations, *J. Geophys. Res. Space Physics*, *118*, 5592–5602, doi:10.1002/jgra.50529.
- Prangé, R., D. Rego, L. Pallier, J. E. P. Connerney, P. Zarka, and J. Queinnee (1998), Detailed study of FUV Jovian auroral features with the post-COSTAR HST faint object camera, *J. Geophys. Res.*, *103*(E9), 20,195–20,215, doi:10.1029/98JE01128.
- Pryor, W. R., et al. (2011), The auroral footprint of Enceladus on Saturn, *Nature*, *472*, 331–333.
- Radioti, A., D. Grodent, J.-C. Gérard, E. Roussos, C. Paranicas, B. Bonfond, D. G. Mitchell, N. Krupp, S. Krimigis, and J. T. Clarke (2009), Transient auroral features at Saturn: Signatures of energetic particle injections in the magnetosphere, *J. Geophys. Res.*, *114*, A03210, doi:10.1029/2008JA013632.
- Ray, L. C., Y.-J. Su, R. E. Ergun, P. A. Delamere, and F. Bagenal (2009), Current-voltage relation of a centrifugally confined plasma, *J. Geophys. Res.*, *114*, A04214, doi:10.1029/2008JA013969.
- Ray, L. C., M. Galand, L. E. Moore, and B. Fleshman (2012), Characterizing the limitations to the coupling between Saturn's ionosphere and middle magnetosphere, *J. Geophys. Res.*, *117*, A07210, doi:10.1029/2012JA017735.
- Ray, L. C., M. Galand, P. A. Delamere, and B. L. Fleshman (2013), Current-voltage relation for the Saturnian system, *J. Geophys. Res. Space Physics*, *118*, 3214–3222, doi:10.1002/jgra.50330.
- Rego, D., R. Prangé, and J.-C. Gérard (1994), Auroral Lyman  $\alpha$  and H<sub>2</sub> bands from the giant planets: 1. Excitation by proton precipitation in the Jovian atmosphere, *J. Geophys. Res.*, *99*(E8), 17,075–17,094, doi:10.1029/93JE03432.
- Rego, D., R. Prangé, and L. Ben Jaffel (1999), Auroral Lyman  $\alpha$  and H<sub>2</sub> bands from the giant planets: 3. Lyman  $\alpha$  spectral profile including charge exchange and radiative transfer effects and H<sub>2</sub> color ratios, *J. Geophys. Res.*, *104*(E3), 5939–5954, doi:10.1029/1998JE900048.
- Schippers, P., M. Moncuquet, N. Meyer-Vernet, and A. Lecacheux (2013), Core electron temperature and density in the innermost Saturn's magnetosphere from HF power spectra analysis on Cassini, *J. Geophys. Res. Space Physics*, *118*, 7170–7180, doi:10.1002/2013JA019199.
- Tao, C., S. V. Badman, and M. Fujimoto (2011), UV and IR auroral emission model for the outer planets: Jupiter and Saturn comparison, *Icarus*, *213*, 581–592.
- Waite, J. H., Jr., T. E. Cravens, J. Kozyra, A. F. Nagy, S. K. Atreya, and R. H. Chen (1983), Electron precipitation and related aeronomy of the Jovian thermosphere and ionosphere, *J. Geophys. Res.*, *88*(A8), 6143–6163, doi:10.1029/JA088iA08p06143.
- Waite, J. H., Jr., J. T. Clarke, T. E. Cravens, and C. M. Hammond (1988), The Jovian aurora: Electron or ion precipitation?, *J. Geophys. Res.*, *93*(A7), 7244–7250, doi:10.1029/JA093iA07p07244.
- Yung, Y. L., G. R. Gladstone, K. M. Chang, J. M. Ajello, and S. K. Srivastava (1982), H<sub>2</sub> fluorescence spectrum from 1200 to 1700 Å by electron impact: Laboratory study and application to Jovian aurora, *Astrophys. J.*, *254*, L65–69.